Chaotic passive micromixers with microstructures placed on the top and bottom floors of channel

J. J. Chen*[a], Y. R. Lai[b], J. D. Lin[b]
[a] Department of Biomechatronics Engineering, National Pingtung University of Science and Technology, 1, Hseuh Fu Road, Nei Pu, Pingtung 912, Taiwan, ROC;
[b]Dept. of Mechanical Engineering, National Chiao Tung University, 1001 Ta Hsueh Rd., Hsinchu, Taiwan 300, ROC

ABSTRACT

The objective of this study is to present chaotic micromixers in which a series of microstructures are placed on the top and bottom floors of channels. Passive micromixers fabricated by MEMS technologies with crosswise grooves and ridges are considered. Numerical simulations using the commercial software CFD-ACE(U) are employed to predict the effects of various patterns of microstructures on mixing efficiency with the range of Reynolds number from 0.05 to 50. The influences of non-dimensional parameters such as the Reynolds number as well as the geometrical parameters on the mixing performance are presented in terms of the mixing index. Micromixers which are made of PDMS are used to investigate the mixing characteristics influenced by the different kinds of microstructures. A significant amount of stirring resulting from chaotic mixing can be seen due to the fluids flowing through the crosswise ridges embedded on the top and bottom floors of channels. While Re is greater than 1, the mixing index of the micromixer with crosswise ridges starts to increase as Re increases. This means that the flow field in this micromixer results in efficient chaotic mixing. Simulation results are presented to compare with the experimental data, and a very good agreement can be achieved. Finally, various numbers of the crosswise ridges with the same orientation in one cycle of the channels are investigated to present to the mixing performance in the microchannels. An optimal design can be found in our works.

Keywords: top and bottom floors, crosswise ridges, cycle.

1. INTRODUCTION

In the last decade, microfluidic technologies have been one of the most interesting topics that span several disciplines. Some products have been mass-production using MEMS. Microfluidic devices ensuring homogenization of solutions of reagents have been developed for a broad range of applications. Effective mixing is important in many miniaturized multi-component flow systems. Fast mixing can reduce the analyzing time and improve reaction efficiency in industrial applications. Traditionally, both stirring and creation of turbulent flow are exploited to improve the mixing characteristics in macroscopic world. In micro-scale system, the dimensions are too small that Reynolds numbers exceeding 1000 are not feasible and only a laminar and uniaxial flow of the liquid can be observed (Reynolds number indicates the ratio of inertia to viscous forces and is expressed as $Re=U_{in}W/\nu$ with U_{in} being the inlet flow velocity and W the width of the microchannel. ν is the kinematic viscosity.). So rapidly mixing in microfluidic analytical devices cannot be achieved by convectional methods. In a typical microfluidic device, the mixing of two or more fluid streams is by virtue of molecular diffusion which is driven by a concentration difference and is a rather slow process. Based on Fick's law, diffusion speed increases with the rise of the contact surface of two liquids [1]. Besides the time taken when molecules travel or diffuse is increasing in proportion to the square value of the distance and further depends on the diffusivity of the diffusing compound [2]. In order to speed up mixing, the essentials of a micromixer based on diffusion are, therefore, the maximization of the contact area of different fluids and the minimization of the diffusing distance. Among these technologies a number of micromixers have been developed. These can be classified into two groups: active and passive micromixers. Though the time and length of the channel required for active mixing are less than for passive mixing, the active micromixers are difficult to fabricate, clean and integrate into microfluidic systems. The pronounced advantage of passive micromixers is that utilize no external power except the mechanism used to drive the fluids into the microfluidic systems. During the period, studies of passive mixing in micromixers have been conducted. Nguyen and Wu presented

Microfluidics, BioMEMS, and Medical Microsystems VI, edited by Wanjun Wang, Claude Vauchier,
Proc. of SPIE Vol. 6886, 68860I, (2008) · 0277-786X/08/$18 · doi: 10.1117/12.761971

an elaborate review for the micromixers, and reported the progress on the recent development of micromixers [3]. Since there is difficult to generate the turbulent liquid flow on the microscale, mixing in passive micromixers relies mainly on molecular diffusion and chaotic advection. By considering the characteristics of molecular diffusion, some have dealt with the injection mixing when the liquid fluid injects into the other with micro plumes [4, 5] or some studies proposed the micromixers based on the increase of the boundary surface with the concept of lamination [6, 7]. These designs split the incoming streams into several narrower confluent streams and rejoin them together. Then the thickness of each fluid layer which is greatly reduced is comparison with the characteristic diffusion length, and it reduces the mixing equilibration time. Although the flow splitting technique is effective, it is still limited by diffusion. These kinds of micromixers need enough space to separate fluids into several channels in order to mix fluids rapidly and may result in a higher pressure drop. To increase the mixing rate beyond diffusion limited, it is necessary to induce off-axis or lateral transport within the channel [8]. Fortunately, mixing in such laminar flows can be enhanced through chaotic advection [9]. A chaotic mixer refers to unit operation that involves stretching and folding of the fluid volumes over the cross section of the channel [10]. Dynamic systems theory shows that chaotic advection can occur when a velocity field is either two-dimensional with time dependent perturbation or three-dimensional with or without time dependent. The occurrence of chaotic advection typically results in enhanced transverse flow, and indicates rapid distortion and elongation of material interfaces. This deformation significantly increases the interfacial area across which diffusion occurs, which leads to rapid mixing. Some researches achieved the flow phenomenon in their microstructures by using three-dimensional twisted channels [11], electrokinetic instability [12], or bas-relief structure on the floor of the channel [13]. The challenges of three-dimensional twisted channels are the micro-fabrication of complex structures and the need for high Reynolds number to stir the fluids to generate chaotic advection. Besides the micromixer by using electrokinetic instability is an active micromixer with no moving parts that take advantage of fluctuating electric fields to effect mixing, and a function generator coupled with a high-voltage amplifier is needed to provide the fluctuating electric fields. So to create transverse flows in microchannels that can be used to induce chaotic stirring at a wider range of Reynolds number is to place some bas-relief structures on the floor of the channels.

Stroock et al. [13] initially developed two different micromixers with bas-relief structures. One is a slanted groove mixer (SGM) in which ridges on the floor of the channel at an oblique angle with respect to the long axis of the channel and the other is a staggered herringbone mixer (SHM) in which a series of asymmetric herringbone grooves are etched onto the channel floor to improve the mixing efficiency. The major mixing mechanism might be splitting and reorientation due to periodic up- and down-welling motion. Johnson et al. [9] proposed an effective chaotic SGM, whereby slanted grooves at a 45 degree angle and/or a series of partial slanted grooves are placed on the floor of the channel. In this mixer there induces a high degree of lateral transport across the channel over a broad range of electroosmotic flow rates. Then some researchers numerically and/or experimentally analyzed these two micromixers for characterizing the mixing assessment. And both qualitative and quantitative techniques were reported for describing the flow fields and mixing mechanisms in the channels. The influence of various geometric parameters of micromixers on the mixing characteristics was also investigated [14-21]. Bhagat et al. [22] developed a passive mixer containing diamond obstructions along the channel centerline and triangular notches in the sidewall. Due to the symmetric obstructions inside the mixer, results did not show complete mixing. To improve the mixing performance in the micromixers, researchers introduced the micromixers with patterned grooves or ridges on both the top and bottom of the channel. Schonfeld and Hardt [23] studied the helical flows in bas-relief structured SGM. It was shown that bas-relief structures on two opposite walls lead to a significant increase of the relative transverse velocity compared to channels with structures on only one wall. Howell et al. [24] also presented a microfluidic mixer containing chevron and stripe grooves on both the top and bottom of the channel. This design created vertically stacked vortices as well as two vortices positioned side by side. For comparison with the SHM, this mixer achieved superior mixing. Kim et al. [25] studied barrier embedded micromixers (BEM) in which barriers are periodically inserted along the top surface of the channel and slanted grooves are placed on the bottom surface. They established that the flow field in the BEM has one hyperbolic point in the velocity field of co-rotating cross-sectional flows, which inherently causes tremendous stretching around it, thereby resulting in very efficient chaotic mixing [10]. Kang and Kwon [26] applied the colored particle tracking method to three representative patterned groove micromixers: SGM, SHM and BEM. The results show that there is no notable chaotic mechanism in the case of the SGM as opposed to the other two micromixers.

In all of the aforementioned studies, two representative patterned groove micromixers (SGM and SHM) were discussed detailedly. In the case of SGM, the previous results showed that there exists the poorer mixing compared with the case of SHM since one way to produce a chaotic flow is to subject volumes of fluid to a repeated sequence of rotational and extensional local flows [14]. For high aspect ratio grooves, the flow pattern becomes more jumbled than for small aspect ratio grooves, but there is no apparent evidence that indicates the flow is chaotic, for Reynolds numbers up to five [16].

However, when the barriers are periodically placed built or the slanted grooves can be patterned on the top surface of the microchannel in the micromixers. The stronger the helical flow becomes, the higher the order of mixing that can be achieved [25]. Referred to the previous works, bas-relief structures on two opposite walls lead to a significant increase of the mixing performance. However, few researchers investigated the influence of various geometric parameters of a SGM on the mixing characteristics.

The objective of the present study is to demonstrate a designed chaotic micromixer in which a series of crosswise ridges or grooves are etched onto the top or bottom floors of channel which is fabricated using MEMS technology. A helical flow was realized by slanted patterns which were fabricated onto the top or bottom floors of microchannels. A three-dimensional fluid field is used to describe the flow characteristics in the micro system. The effects of non-dimensional parameters such as the Reynolds number, based on the inlet velocity on flow characteristics are examined. Flow experiments are performed and compared with the results of numerical simulations. Finally, the influences of the number of the crosswise ridges with the same orientation for a cycle along the downchannel on the mixing process are presented in terms of the mixing characteristics.

2. MATHEMATICAL MODEL AND NUMERICAL METHODOLOGY

In this study, the mixing characteristics of two liquids entering the two top branches of a crosswise grooves micromixer, subjected to a specific inlet pumping velocity at various values of geometrical and/or operational parameters are examined. The numerical simulations are performed for the mixing performance of different kinds of liquid flows inside the microchannels. It is assumed the variations of the concentration do not modify the viscosity and the density of the fluid; the channel walls are assumed to be smooth; and the wall surface tension forces are neglected.

The governing equations consist of conservation equations of mass and momentum, and species. The conservation equations of mass and momentum are solved to determine the flow field of the liquids. The conservation equation of mass, also known as the continuity equation or the law of conservation of mass, states that the rate of accumulation of mass per unit volume plus the net flow rate of mass efflux per unit volume are zero. In symbolic notation, the continuity equation can be expressed as follows

$$\nabla \cdot \vec{U} = 0 \tag{1}$$

where $\vec{U}$ is the fluid velocity vector.

The momentum equation for a continuum is the analogue of Newton's second law for a point mass. The momentum principle is the time rate of change of the linear momentum of a material region is equal to the sum of the forces on the region. In symbolic notation the momentum equation is

$$\nabla \cdot \left(\rho \vec{U} \vec{U}\right) = -\nabla P + \nabla\left(\mu \nabla \vec{U}\right) \tag{2}$$

where P is the pressure and μ is the fluid viscosity.

Species transport by pressure-driven flows occurs as a result of convection and diffusion and can be described by the combined species convection-diffusion equation. Fick's second law is used in non-steady or continually changing state diffusion, i.e., when the concentration within the diffusion volume changes with respect to time. In symbolic notation the momentum equation is

$$\nabla \cdot \left(\rho \vec{U} \phi\right) = \nabla\left(D \nabla \phi\right) \tag{3}$$

where D is the mass transfer coefficient, and ϕ is the mass concentration. This equation must be solved together with Eqs. (1) and (2) in order to achieve computational coupling between the velocity field solution and the concentration distribution.

A computational fluid dynamics package (CFD-ACE+, CFD Research Corporation, CA, USA) using a finite element approach is utilized to solve three dimensional flow fields as well as two-fluid mixing. A nonlinear steady-state algorithm is used for hydrodynamic calculations, and a linear steady-state one is used for the solving of the diffusion-convection equation. Three dimensional structured grids are employed, and the SIMPLEC method is adopted for pressure-velocity coupling, and then all spatial discretizations are performed using the first-order upwind scheme. The simulation is implemented in steady state. A fixed-velocity condition is set to the boundary at the inlet of the mixer, and the boundary condition at the outlet is set at a fixed pressure. The concentration of species is normalized to be one and zero for the inlet in the right side and left side, respectively. The fluid properties are set to the physical and thermodynamic properties of water at 300K. The solution is considered to be converged when the relative error of all dependent variables are less than 10^{-4} between the sweeps n and n+1.

In the present study, we consider some different configurations of the flow system. The general configuration consists of

some slanted ridges and/or grooves on the top and bottom floors (c.f. Fig. 1). The grid systems of the computation domain are chosen to assure the orthogonality, smoothness and low aspect ratios to prevent the numerical divergence. Poor orthogonality most directly affects the accuracy of the flux calculations, while poor smoothness and high aspect ratios most directly affect the accuracy of the surface reconstruction.

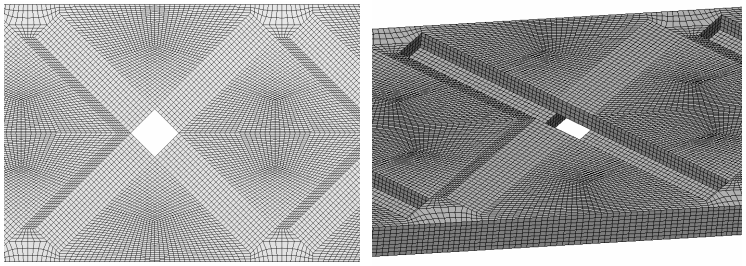

Figure 1. The grid system of the computational domain.

An analysis of the grid size sensitivity has been conducted at the very beginning and shown in Table 1. The middle case has been chosen for further investigation such that the mixing indices of the three different places are almost the same.

Table 1 Grid sensitivity analysis

		Mixing index		
Numbers of edges	Number of nodes	x=0.065 cm	x=0.951 cm	x=1.842 cm
80x1800	724425	10.49%	36.16%	53.79%
86x1900	824040	10.33%	36.09%	53.71%
90x2000	908600	10.23%	36.04%	53.68%

The uniformity of the mixing at sampled sections is evaluated by checking the mixing index φ of the solute concentration which is defined as

$$\varphi = 1 - \frac{I_D}{I_{pm}} \tag{4}$$

and

$$I_D = \sqrt{\frac{1}{N}\sum_{i=1}^{N}\left(I_i - I_{pm}\right)^2} \tag{5}$$

which I_D is the normalized deviation from the fully mixed state. I_i is the concentration value (between 0 and 1), I_{pm} is the averaged value of the concentration over the sampled section (Here we take I_{pm} as the value of 0.5). The mixing index φ ranges from 0 for non-mixing to 1 for complete mixing.

3. FABRICATION PROCESS AND FLOW VISUALIZATION

For the purpose of experimental characterization of the mixing performance of chaotic passive micromixers, different types of microchannels are fabricated: a microchannel having only crosswise grooves and a microchannel having slant grooves or ridges on the top and bottom floors of channels. The flow device is fabricated by a replica molding method. The microfabrication process is schematically illustrated in Fig. 2 and 3. Initially, silicon wafers are cleaned as shown in Fig. 2(A). A thin film is fabricated by spin coating of negative photoresist (SU8) on silicon wafers as shown in Fig. 2(B) and the channel pattern is fabricated by photolithography using a chrome photo mask as shown in Fig. 2(C). The wafer with patterned SU-8 is then obtained as shown in Fig. 2(D).

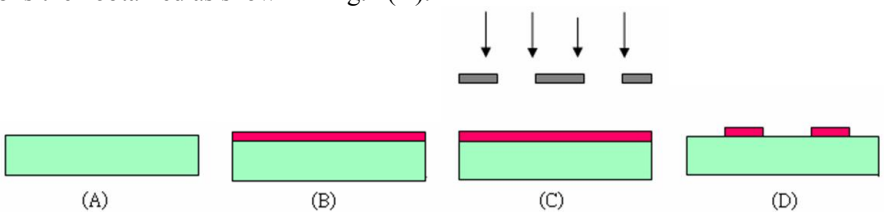

Figure 2. Schematic diagram illustrating the microfabrication process of the SU-8 molds.

The wafer is rinsed in DI water and dried with nitrogen as shown in Fig. 3(A). After pouring the PDMS on the wafer with patterned SU-8, upper and lower plate structures are fabricated by a PDMS (polydimethylsiloxane) molding process using a SU-8 mold as shown in Fig. 3(B). The microchannels are designed by forming molds of upper and lower plate structure using conventional planar lithography. Methanol is used as a surfactant to prevent two oxygen plasma treated PDMS replicas from being bonded irreversibly without proper alignment. After O_2 plasma treatment and bonding, finally we fabricate micromixers that have 3D microchannels. In Fig. 3(C), it shows a designed chaotic micromixer in which a series of crosswise ridges were etched onto the bottom floor of channel. And a series of crosswise ridges are etched onto the top and bottom floors of channel as shown in Fig. 3(D).

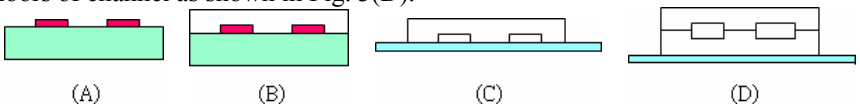

Figure 3. Schematic diagram illustrating the microfabrication process of the PDMS micromixers.

Figure 4 shows the SEM pictures of the microchannel for one typical version of micromixers realized in this study. The width, thickness and length of the microchannels are 750 μm, 45 μm and 4 cm, respectively, for all three microchannels. The grooves or ridges are 100 μm long, 15 μm deep.

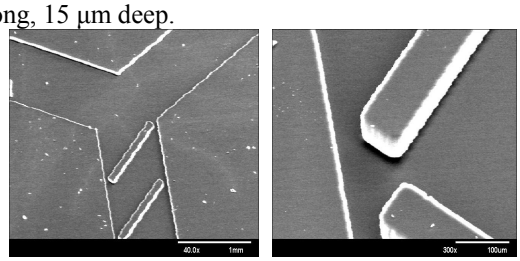
Figure 4. The SEM pictures of the microchannel.

For the mixing experiment in pressure-driven flow, two different fluids are injected into microchannels by a syringe pump (KD Scientific, Programmable Syringe Pump) at a preset constant flow rate. The experimental setup for testing performances of fabricated micromixers is shown in Fig. 5. One syringe is loaded with the DI water; the other is loaded with the colorful ink. The working fluids enter into inlet channels, flow through the micromixer, and finally go out through an outlet channel. In order to investigate the effect of the mixing processes on the mixing performance, several experiments are carried out with various flow rates for different micromixers. Once the steady state is reached, the color change along the downchannel direction is captured by means of a microscope and a high speed camera (IDT, X-Stream High-Speed Cameras, XS-4) at 40 × magnifications with a graphic grabber system (VCD-Gear TV Plus). Images are analyzed using image processing software (MyImgPro). Gray-scale values across the channel width at different locations are used to determine the relative amount of mixing.

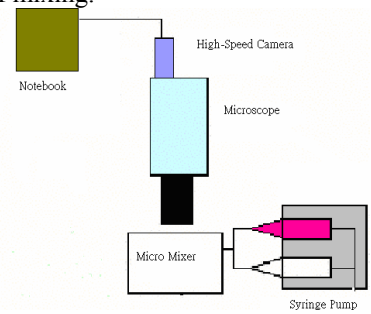

Figure 5. Experimental setup.

We normalize the color intensities of pictures, taken in experiments of each micromixer, using equation (6) to get the normalized color intensity of a pixel.

$$I_{ni} = \frac{I_i - I_{\min}}{I_{\max} - I_{\min}} \tag{6}$$

where I_{min} is the minimum intensity of a pixel that is measured from the mixer when the DI water flows into two inlets.

I_{max} is the maximum intensity of a pixel that is measured from the mixer when the ink-water solution flows into two inlets. I_i is the color intensity of a pixel. And I_{ni} is the normalized color intensity of a pixel. Then the uniformity of the mixing at sampled sections is evaluated by checking the mixing index φ of the solute concentration which is the same as Eq. (4) and (5), except that I_i is replaced by I_{ni}. The mixing index also ranges from 0 for non-mixing to 1 for complete mixing. The micromixers are designed to investigate the influences of various parameters such as Reynolds number and Peclet number on the mixing characteristics associated with the geometric dimension effect.

4. RESULTS AND DISCUSSION

In the follows, we consider two different configurations of the microfluidic system experimentally. The microchannels were of 750 μm in width, 45 μm in depth and 4 cm in length. The experimental mixing results of each micromixer are taken at five representative positions, 0, 1, 2, 3, and 4 cm beyond the Y-junction, along the downchannel direction. The influences of the various parameters on the flow fields and mixing characteristics inside the microfluidic system are examined first. And then the effects of the changes in crosswise ridges on the floors of microchannels are investigated. The parameters of above values are used unless otherwise specified.

In this work, we additionally design a micromixer with a straight channel to verify the performance of the crosswise ridge mixer. Fig. 6 shows the experimental mixing results of each micromixer at five representative positions along the downchannel direction when DI water and ink-water solution are injected through each inlet at an input flow rate of 100 μl/min, which corresponds to the inlet flow velocity of 0.05 m/s and Reynolds number of 10. In the case of the Y-type mixer, two streams flowing in parallel meet each other exactly at the center of the channel and thus the interface is clearly observed in the front part of the channel as shown in Fig. 6(A). It shows the flow field in this channel is essentially a laminar flow till the end of the channel. The mixing of two fluids is only through molecular diffusion across the interface of the two liquid species. Fig. 6(B) shows that the designed mixer with crosswise grooves on the bottom floors has a very little improvement in mixing between the two fluids in the microchannel, and the interface of two fluids is not clearly observed as shown in Fig. 6(A). This is because that the distortions are caused by the microstructures on the bottom floor or maybe the velocities of two inlets are a little different. However, this is not clear that the mixing process can be achieved very quickly, since the crosswise grooves on the bottom floors are symmetric with the central line of the microchannel. It is clear from Fig. 6(C) that the mixed fluids are well dispersed across the channel. The microchannel was of 90 μm in depth. And mixing is improved by placing the slanted ridges on the top and bottom floors due to the stretching and folding of the fluids.

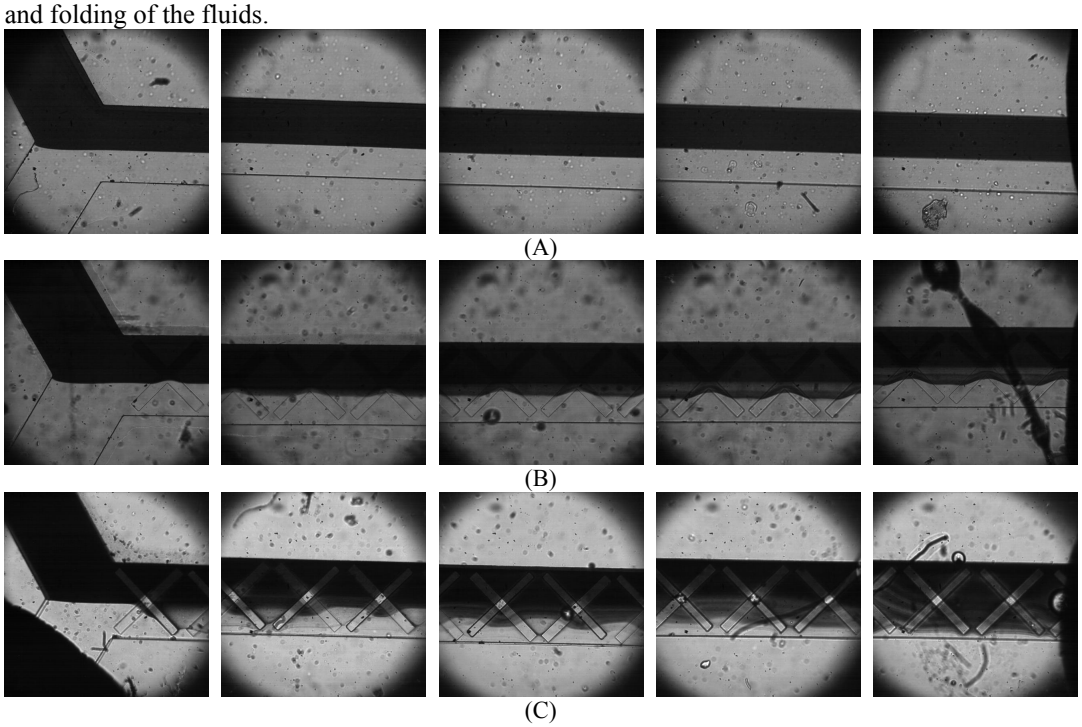

(A)

(B)

(C)

Figure 6. Photographs of mixing experimental results of (A) Y-type mixer, (B) crosswise groove mixer with crosswise grooves on the bottom floors and (C) crosswise ridge mixer with slanted ridges on the top and bottom floors for Re=10.

The numerical mixing characteristics of the above micromixers are shown in Fig. 7. The flow conditions are the same as the cases in Fig. 6 except for the crosswise groove mixer with crosswise grooves on the bottom floors. In Y-type mixer, two fluids meet each other at the centerline along the downchannel in Fig. 7(A). This result is the same as the results shown in Fig. 6(A). The crosswise grooves of the crosswise groove mixer are symmetric with the central line and the mixing performance will be similar to the results shown in Fig. 7(A) when the inlet velocities of two fluids are equal. However, the interface of two fluids is not clearly observed and the mixing is enhanced a little bit in Fig. 7(B). It's because the velocities of two inlets are a little different. The fluid with larger inertia force can push the other fluid away from the central line of the channel and the interface of two fluids is no longer coincident with the symmetric axis. Then a little enhancement of mixing performance can be seen. The slanting direction of the ridge at the top floor is from left to right and that at the bottom floor is from right to left. The fluid flows along the ridge and then down the ridge. The contact areas of two fluids increase and the diffusion distance decreases. The mixing can rise in a larger value and it can be seen in Fig. 7(C).

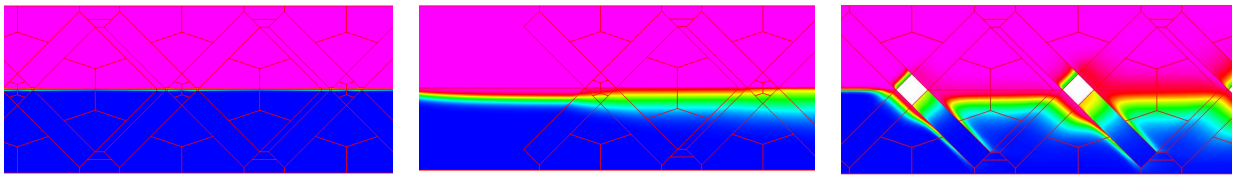

(A) (B) (C)

Figure 7. Numerical mixing results of (A) Y-type mixer, (B) crosswise groove mixer with crosswise grooves on the bottom floors and (C) crosswise ridge mixer with slanted ridges on the top and bottom floors.

Figure 8 shows experimental results using crosswise ridge mixer with ridges on the top and bottom floors at five representative positions along the downchannel direction. The influences of various inlet velocities on the mixing characteristics are plotted. Reynolds numbers, equal to 0.05, 0.1, 1, 10 and 50, are considered, which correspond to the inlet flow velocities of 0.00025, 0.0005, 0.005, 0.05 and 0.25m/s. Figure 8 for the case of Re equal to 50 indicates that good mixing at the end of the channel have been successfully achieved. The interface between streams is indistinct as it moves downstream. By the naked eye, one can obviously tell that the mixing rate in the channel increases with increasing Reynolds number.

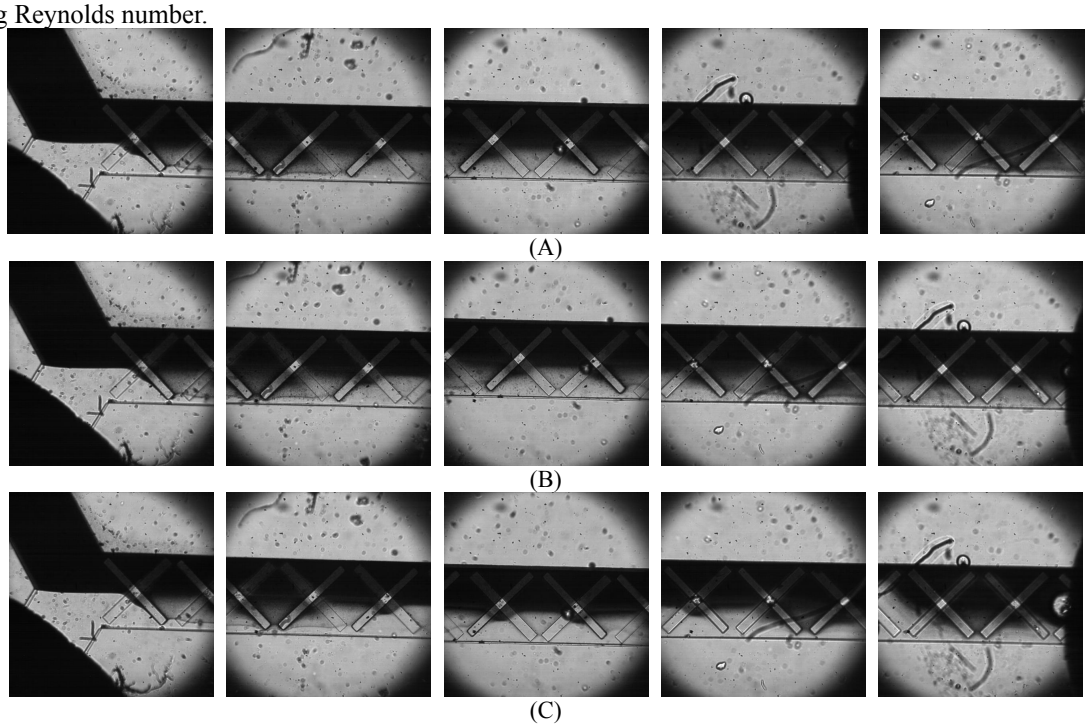

(A)

(B)

(C)

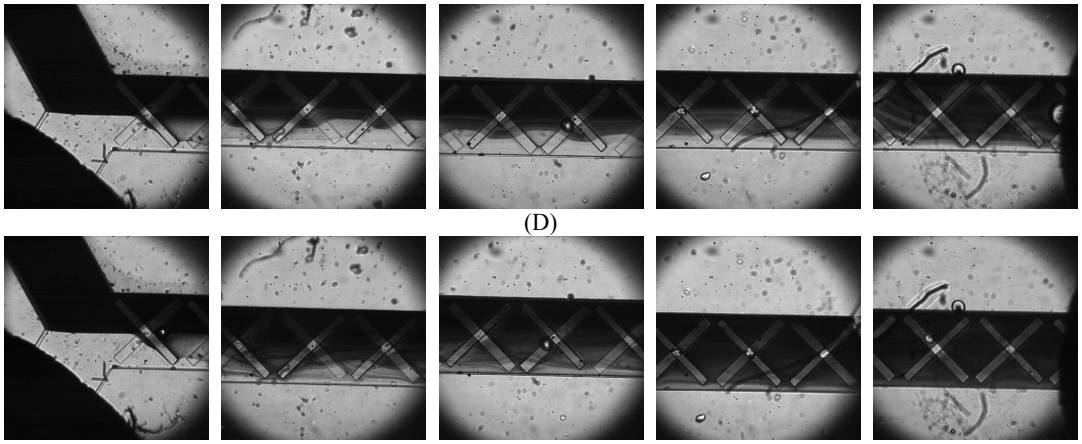

Figure 8. Photographs of mixing experimental results of crosswise ridge mixer with slanted ridges on the top and bottom floors for (A)Re=0.05, (B)Re=0.1, (C)Re=1, (D)Re=10, and (E)Re=50.

The experimental mixing capability of the crosswise ridge mixer with ridges on the top and bottom floors, based on Eq. (6), at several values of Re is quantified in Fig. 9 by comparing with the numerical results. Each normalized intensity value was plotted at the abscissa corresponding to the different Reynolds numbers. At the low Reynolds numbers, 0.01<Re<1, viscous forces in the fluid are large as compared to inertia forces, and the inertia can be neglected. Fluid velocity in a channel cross section is essentially two-dimensional, and the flow creeps through the ridged or grooved channels. Therefore, there is no convective acceleration and the interface is not distorted but only the position of fluids is changed. Mixing is dominated by pure molecular diffusion. Then the mixing index for all mixers decreases as the Reynolds number increases. In the region of Reynolds numbers between 1 and 100, both viscous and inertia forces are important. As a result, flow around a groove or ridge will be three-dimensional, with secondary flows being generated in the channel cross section in addition to the bulk flow along the axis of the channel. These secondary flows, in combination with the axial flow, distort and stretch material interfaces and can produce chaotic advection. As a result, the interfacial area across which diffusion occurs is greatly increased, which leads to rapid mixing. In the micromixers with slanted ridges on the top and bottom floors, mixing increases rapidly as Re increases due to the chaotic advection. The simulated results are also plotted in Fig. 9 and used to make a comparison with the experimented results. Results show the normalized average intensity changing at various Reynolds numbers. As shown in Fig. 9, mixing intensity decreases as Re increases within the ranges of Re between 0.01 and 1. In the region of Reynolds numbers between 1 and 100, as a result of chaotic advection, mixing performance increases as Re increases for the micromixer with slanted ridges on the top and bottom floors. The results between experimental and numerical data are not identical, but are very similar.

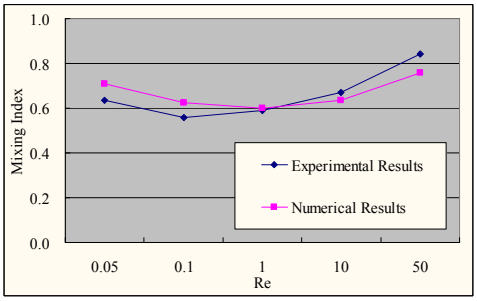

Figure 9. Experimental and numerical mixing index in each channel for various Reynolds numbers.

The velocity vectors changes along the downchannel viewing from the outlet are shown in Fig. 10(A), which corresponds to the inlet flow velocity of 0.05 m/s and Reynolds number of 10. The flow field has two components along the channel. One is the downchannel flow component, and it can be seen as some dots shown in figure. And the other one is the transversely rotational flow components, and two counter wise flow patterns are presented. These two components result in an overall helical flow inside the microchannel. Thus the helical flow achieves superior mixing. The void bottom areas in the images represent the solid part of the micromixer. The simulation mixing results at four cross-section areas along the channel are shown in Fig. 10(B). The transversely rotational flow pushes one fluid to the

other part of the channel which is originally occupied by the other fluid. These images show the stretching and folding of two fluids and the mixing can be improved.

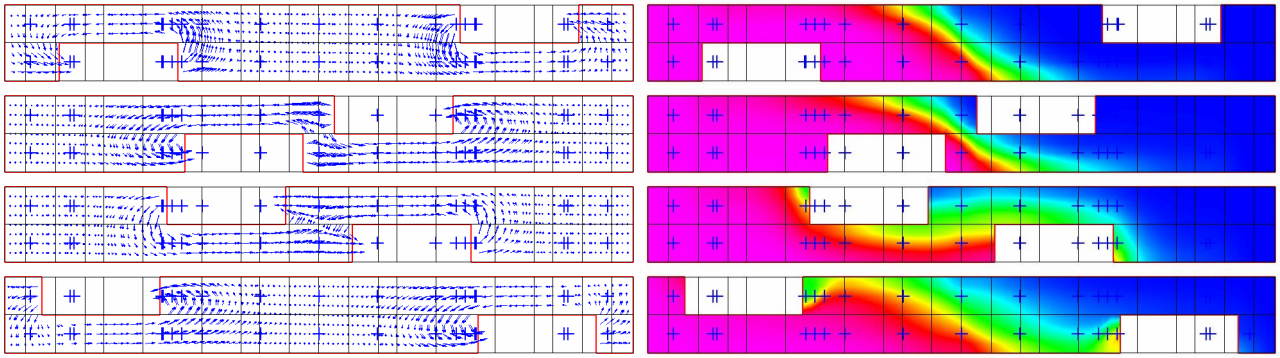

(A) (B)

Figure 10. (A) The vector planes and (B) the mixing characteristics at four cross-section areas along the down channel.

A mixing cycle is composed of two consecutive regions of ridges; the direction of the slanting direction of the ridges switches with respect to the centerline of the channel from one region to the other. Sixteen, eight, four and two ridges are placed on the floors in one cycle are represented in Fig. 11(A), 11(B), 11(C) and 11(D), and the mixing index is 0.74, 0.69, 0.61 and 0.44, respectively, at Reynolds number equal to 50. The orientations of the ridges keep the same in half a cycle. One fluid flows along and down the ridges, and can be directed to the other part of the channel, shown in Fig. 11(A). It enhances mixing performance. The more ridges in one cycle, the higher mixing index are achieved. The mixing index is 0.75 for sixteen ridges placing in half a cycle shown in Fig. 9. And then the mixing performance achieves to a maximum value as the number of the ridges in one cycle is equal to eight. The switch of the slanting direction of the ridges redirects the fluids toward the centerline of the channel. The fluids are directed to the other part of the channel and then soon redirected back to the original part when the number of the ridges in one cycle is equal to. This means less contact areas are provided along the downchannel, poor mixing is achieved.

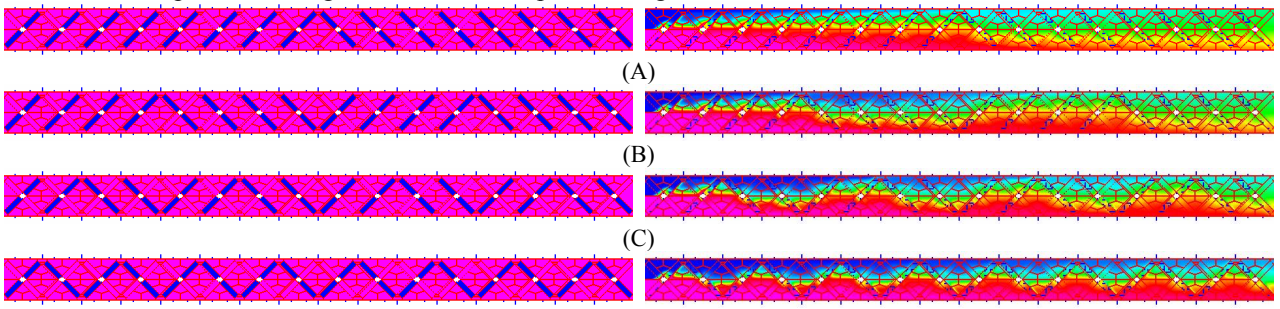

(A)

(B)

(C)

(D)

Figure 11. The mixing characteristics for various numbers of the crosswise ridges with the same orientation in one cycle of the channels

5. CONCLUSIONS

In the present study, we have demonstrated the mixing characteristics of two fluids in a crosswise grooves or ridges micromixer by numerical studies associated with the micro channels with various inlet velocities which is fabricated in PDMS by standard MEMS technology and covered by a Pyrex glass chip through bonding technology. A three-dimensional computational model is proposed to perform the mixing of two fluids. The results are presented in terms of the distributions of the concentrations. Fluid flow simulations are performed to investigate the mixing index of the liquid fluids and/or the velocity vectors at the cross-section regions. For the microchannels with the crosswise ridges at the top and bottom floors, the downchannel flows and the transvesely rotational flows result in helical flows along the downchannel. It is clear that the mixing performance is significantly influenced by the chaotic advection flow is also dependent upon the values of Reynolds number. Experimental results show that micromixer with crosswise ridges embedded on the top and bottom floors of channels has great mixing efficiency and the mixing index increases 82% when the Reynolds number is about 50. The numerical results are also compared with experimental measurements and

show good agreements in the distributions of the concentrations and the mixing index of two fluids. Finally, the effects of the various numbers of the crosswise ridges with the same orientation in one cycle of the channels are also studied. The above-mentioned geometric changes significantly affect the mixing phenomenon of liquids in the micro channel. It is evident that the orientations of the ridges have considerable effects on the direction of the fluids and the mixing performance achieves to a maximum value as the number of the ridges in one cycle is equal to eight.

REFERENCES

1 F. P. Incropera and D. P. De Witt, *Fundamentals of Heat And Mass Transfer*, 3rd edn., John Wiley & Sons, New York, 1990.
2 E. L. Cussler, *Diffusion Mass Transfer in Fluid Systems*, Cambridge Univ. Press, New York, 1984.
3 N. T. Nguyen and Z. Wu, *J. Micromech. Microeng.*, 2005, **15**, R1.
4 R Miyake, T. S. J. Lammerink, M. Elwenspoek and J. H. J. Fluitman, *Micro mixer with fast diffusion*, Proc.s MEMS'93, 6th IEEE Int. Workshop Micro Electromechanical System, San Diego, C*A,* 1993, p. 248.
5 J. Voldman, M. L. Gray and M. A. Schmidt, *J. Microelectromech. Syst.*, 2000, **9**, 295.
6 H. Mobius, W. Ehrfeld, V. Hessel and T. Richter, *Sensor Controlled Processes in Chemical Microreactors*, Proc. Transducers '95, 8th Int. Conf. on Solid-State Sensors and Actuators, Stockholm, Sweden, 1995, p. 775.
7 J. Branebjerg, P. Gravesen, J. P. Krog and C. R. Nielsen, *Fast Mixing by Lamination*, Proc. MEMS'96, 9th IEEE Int. Workshop Micro Electromechanical System, San Diego, CA, 1996, p. 441.
8 S. W. Jones, O. M. Thomas and H. Aref, *J. Fluid Mech.*,1989, **209**, 335.
9 T. J. Johnson, D. Ross, and L. E. Locascio, *Anal Chem*, 2002, **74**, 45.
10 J. M. Ottino, *The Kinematics of Mixing: Stretching, Chaos, and Transport*, Cambridge Univ. Press, New York, 1989.
11 R. H. Liu, M. A. Stremler, K. V. Sharp, M. G. Olsen, J. G. Santiago, R. J. Adrian, H. Aref and D. J. Beebe, *J. Microelectromech. Syst.*, 2000, **9**, 190.
12 M. H. Oddy, J. G. Santiago and J. C. Mikkelsen, *Anal Chem*, 2001, **73**, 5822.
13 A. D. Stroock, S. K. W. Dertinger, A. Ajdari, I. Mezic, H. A. Stone and G. M. Whitesides, *Science*, 2002, **295**, 647.
14 J. Aubin, D. F. Fletcher, J. Bertrand and C. Xuereb, *Chem. Eng. Technol.*, 2003, **26**, 1262.
15 D. Lim, Y. Kamotani, B. Cho, J. Mazumder and S. Takayama, *Lab Chip*, 2003, **3**, 318.
16 H. Wang, P. Iovenitti, E. Harvey and S. Masood, *J. Micromech. Microeng.*, 2003, **13**, 801.
17 C. Li and T. Chen, *Sens. Actuators, B*, 2005, **106**, 871.
18 J. Aubin, D. F. Fletcher and C. Xuereb, *Chem. Eng. Sci.*, 2005, **60**, 2503.
19 J. T. Yang, K. J. Huang and Y. C. Lin, *Lab Chip*, 2005, **5**, 1140.
20 M. Camesasca, I. Manas-Zloczower and M. Kaufman, *J. Micromech. Microeng.*, 2005, **15**, 2038.
21 D. G. Hasssell and W. B. Zimmerman, *Chem. Eng. Sci.*, 2006, **61**, 2977.
22 A. A. S. Bhagat, G. Dagani, E. T. K. Peterson, J.-H. Lee and I. Papautsky, Microfluidics, BioMEMS. And Medical Microsystems III, Proceedings of SPIE Vol. 5718, Bellingham, WA, 2005, p. 291.
23 F. Schonfeld and S. Hardt, *AIChE J.*, 2004, **50**, 771.
24 P. B. Howell, Jr., D. R. Mott, S. Fertig, C. R. Kaplan, J. P. Golden, E. S. Oran and F. S. Ligler, *Lab Chip*, 2005, **5**, 524.
25 D. S. Kim, S. W. Lee, T. H. Kwon and S. S. Lee, *J. Micromech. Microeng.*, 2004, **14**, 798.
26 T. G. Kang and T. H. Kwon, *J. Micromech. Microeng.*, 2004, **14**, 891.
27 *CFDRC Module Manual*, CFD Research Corporation, 2002.

*Chaucer@mail.npust.edu.tw; phone 886 8 772-3202 ext.7029; fax 886 8 7740420; www.npust.edu.tw